Modelling of Piezoelectric Actuator Dynamics for Active Structural Control

NESBITT W. HAGOOD, WALTER H. CHUNG AND ANDREAS VON FLOTOW

Space Engineering Research Center
Massachusetts Institute of Technology
Cambridge, Massachusetts 02139

ABSTRACT: The paper models the effects of dynamic coupling between a structure and an electrical network through the piezoelectric effect. The coupled equations of motion of an arbitrary elastic structure with piezoelectric elements and passive electronics are derived. State space models are developed for three important cases: direct voltage driven electrodes, direct charge driven electrodes, and an indirect drive case where the piezoelectric electrodes are connected to an arbitrary electrical circuit with embedded voltage and current sources. The equations are applied to the case of a cantilevered beam with surface mounted piezoceramics and indirect voltage and current drive. The theoretical derivations are validated experimentally on an actively controlled cantilevered beam test article with indirect voltage drive.

INTRODUCTION

PIEZOELECTRIC MATERIALS HAVE become increasingly important as sensors and actuators in active structural control applications. In recent years piezoelectric elements have been widely used as actuators in adaptive structures from beams and plates [1–6], to trusses and more complicated structures [7–10]; and as distributed sensors for both modal [11] and wave [12,13] control. Piezoelectric materials possess certain properties which make them useful as sensors or control elements for structures. The first is that they strain when an electrical field is applied across them. This property makes them well suited as actuators for control systems (where the control signal is typically an applied voltage). The second is that they produce a voltage under strain. This property makes them well suited as sensors. In general, piezoelectrics have the ability to transform mechanical energy to electrical energy and vice-versa.

Typically the electrical dynamics of the piezoelectric are ignored when it is used as an actuator and likewise the effect that the piezoelectric has on the structural dynamics is ignored when it is used as a sensor. As applications squeeze ever higher performance from the closed loop systems, the dynamics of the piezoelectric actuator play an increasingly important role. For instance, the capacitance of the piezoelectric can influence the current drain and corresponding saturation of voltage amplifiers, and electrode lead resistance can add critical phase

lag to a control loop. This paper will attempt to address these issues associated with coupling the piezoelectric actuator dynamics to the mechanical system dynamics.

Recently, a new type of passive damping mechanism for structural systems which uses passive circuits shunting the electrodes of the piezoelectric element to dissipate structural strain energy has been developed [14,15]. This paper will expand this concept to encompass the dynamics of an elastic structure piezoelectrically coupled to an actively driven electrical network.

First the governing dynamic equations for a piezoelectric element driven by a voltage or current source and shunted by an arbitrary electrical circuit will be derived and discretized with assumed elastic and electrical field shapes in a Rayleigh-Ritz formulation. Methods will be presented to derive state space models for the coupled piezoelectric-structural system which reflect the actuator dynamics introduced by the passive circuits. When the piezoelectric is driven by a voltage source and there is no passive electrical network, these models reduce to the standard models for piezoelectric actuators [16,17].

A simple example will be analyzed to demonstrate the use of the models. The state space model will be developed for a simple beam with surface bonded piezoceramics whose electrodes are connected through a simple circuit to voltage and current sources. The analytical results from this model will be compared to the experimental data for the open and closed loop response of a piezoelectrically actuated beam.

GENERAL MODEL OF ELECTROELASTICITY: RITZ FORMULATION

In this section the equations of motion for piezoelectrically coupled electromechanical systems will be derived. The general system is represented in Figure 1. It is composed of an elastic body with inclusions of piezoelectric material which are poled and electroded arbitrarily. A Rayleigh-Ritz formulation will be used to derive the equations of motion of the electroelastic continuum. The assumed displacement field shapes within the elastic body and electric
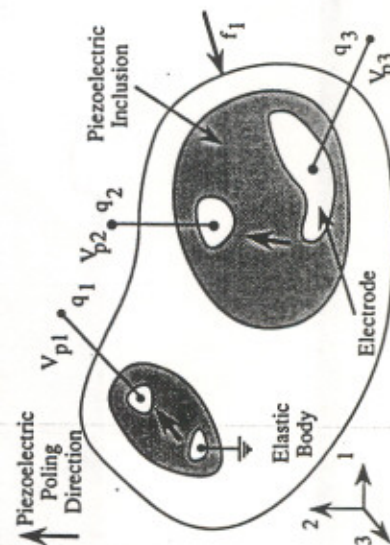

Figure 1. Electroelastic continuum geometry showing piezoelectric inclusions.

potential field shapes about the electrodes will be combined through the piezoelectric properties to form coupled electromechanical equations of motion.

The first step in the derivation is to establish the variational expression for the combined electroelastic body. From Crandall [18] we have a generalized form of Hamilton's principle for coupled electromechanical systems:

$$\int_{t_1}^{t_2} [\partial(T - U + W_e - W_m) + \partial W] dt = 0 \tag{1}$$

for piezoceramics the magnetic terms, W_m, are negligible and the others can be defined:

$$T = \int_{V_e} \frac{1}{2} \varrho_s \dot{u}^T \dot{u} + \int_{V_e} \frac{1}{2} \varrho_p \dot{u}^T \dot{u} \tag{2a}$$

$$U = \int_{V_e} \frac{1}{2} S^T T + \int_{V_p} \frac{1}{2} S^T T \tag{2b}$$

$$W_e = \int_{V_p} \frac{1}{2} E^T D \tag{2c}$$

Contributions to be electrical energy, W_e, due to fringing fields in the structure and free space are neglected. Considering only discrete applied external point forces at locations x_i and applied charges at a discrete set of piezoelectric electrodes:

$$\partial W = \sum_{i=1}^{nf} \partial u(x_i) \cdot f(x_i) - \sum_{j=1}^{nq} \partial \varphi_j \cdot q_j \tag{2d}$$

where $D(x)$ is a vector of electrical displacements (charge/area), $E(x)$ is the vector of electrical field in the material (volts/meter), $S(x)$ is the vector of material strains, $T(x)$ is the vector of material stresses (force/area), $\varphi(x)$ is the scalar electrical potential, $u(x_i)$ is the vector of mechanical displacements, $f(x_i)$ is the vector of applied force at location x_i, and q_j is the charge applied at electrode j. The extension of the work terms to distributed surface or volume forces and charges is straightforward. In terms of their components, these vectors are written:

$$D = \begin{bmatrix} D_1 \\ D_2 \\ D_3 \end{bmatrix}, \ E = \begin{bmatrix} E_1 \\ E_2 \\ E_3 \end{bmatrix}, \ S = \begin{bmatrix} S_{11} \\ S_{22} \\ S_{33} \\ 2S_{23} \\ 2S_{13} \\ 2S_{12} \end{bmatrix} = \begin{bmatrix} S_1 \\ S_2 \\ S_3 \\ S_4 \\ S_5 \\ S_6 \end{bmatrix}, \ T = \begin{bmatrix} T_{11} \\ T_{22} \\ T_{33} \\ T_{23} \\ T_{13} \\ T_{12} \end{bmatrix} = \begin{bmatrix} T_1 \\ T_2 \\ T_3 \\ T_4 \\ T_5 \\ T_6 \end{bmatrix} \tag{3}$$
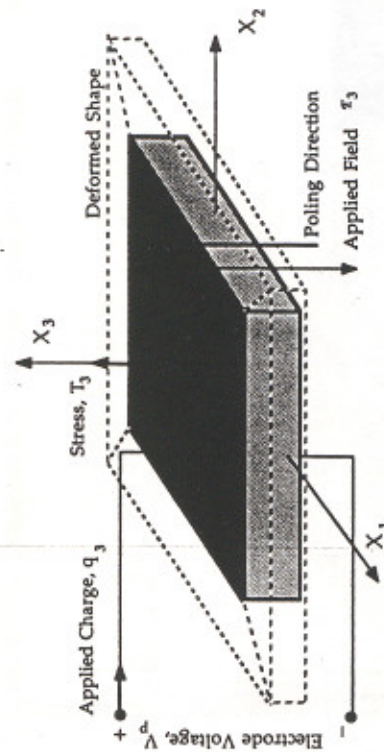
Figure 2. Piezoelectric material directions.

At this point in the derivation of the equations of motion, it is appropriate to introduce the constitutive relations for the structure and the piezoelectric. Within the elastic structure in the global coordinate system, the constitutive relations for the material can be expressed

$$T = c,S \tag{4}$$

For piezoelectrics the properties are defined relative to the local poling direction. For a piezoceramic, the 3 direction is associated with the direction of poling and the material is approximately isotropic in the other two directions. The direction conventions are shown in Figure 2. In the coordinate frame attached to the piezoelectric poling direction, the piezoelectric material properties are given [19,20].

$$\begin{bmatrix} D' \\ T' \end{bmatrix} = \begin{bmatrix} \epsilon^s & e \\ -e_s & c^E \end{bmatrix} \begin{bmatrix} E' \\ S' \end{bmatrix} \tag{5}$$

where the $(\ )'$ denotes variables in the local coordinate frame attached to the poling direction and the subscript $(\ )_s$ denotes transpose. For a piezoceramic the matrix of constitutive properties can be expressed:

$$
\begin{bmatrix} D'_1 \\ D'_2 \\ D'_3 \\ T'_1 \\ T'_2 \\ T'_3 \\ T'_4 \\ T'_5 \\ T'_6 \end{bmatrix}
=
\begin{bmatrix}
\epsilon^s_1 & 0 & 0 & : & 0 & 0 & 0 & 0 & e_{15} & 0 \\
0 & \epsilon^s_1 & 0 & : & 0 & 0 & 0 & e_{15} & 0 & 0 \\
0 & 0 & \epsilon^s_3 & : & e_{31} & e_{31} & e_{33} & 0 & 0 & 0 \\
\cdots & \cdots & \cdots & & \cdots & & & & & \\
0 & 0 & -e_{31} & : & c^E_{11} & c^E_{12} & c^E_{13} & 0 & 0 & 0 \\
0 & 0 & -e_{31} & : & c^E_{12} & c^E_{11} & c^E_{13} & 0 & 0 & 0 \\
0 & 0 & -e_{33} & : & c^E_{13} & c^E_{13} & c^E_{33} & 0 & 0 & 0 \\
0 & -e_{15} & 0 & : & 0 & 0 & 0 & c^E_{55} & 0 & 0 \\
-e_{15} & 0 & 0 & : & 0 & 0 & 0 & 0 & c^E_{55} & 0 \\
0 & 0 & 0 & : & 0 & 0 & 0 & 0 & 0 & c^E_{66}
\end{bmatrix}
\begin{bmatrix} E'_1 \\ E'_2 \\ E'_3 \\ S'_1 \\ S'_2 \\ S'_3 \\ S'_4 \\ S'_5 \\ S'_6 \end{bmatrix}
\tag{6}
$$

where the superscript, $(\ )^s$, signifies that the values are measured at constant strain (e.g., clamped) and the superscript, $(\ )^E$, signifies that the values are measured at constant electrical field (e.g., short circuit). Note that due to symmetry the material properties are identical in the 1 and 2 directions.

The piezoceramics couple the mechanical and electrical equations. In the form of the equations given in Equation (6), the coupling terms are the piezoelectric constants which relate stress to applied field, the e constants. The first term in the subscript refers to the electrical axis while the second refers to the mechanical. Thus, e_{31}, refers to the stress developed in the 1 direction in response to a field in the 3 direction (parallel to the material poling).

Since the e constants and clamped dielectric matrix ϵ^s are sometimes unavailable, they can be expressed in terms of the more commonly available d constants and free dielectric matrix ϵ^T as:

$$e = dc^E \quad \text{and} \quad \epsilon^s = \epsilon^T - dc^E d, \tag{7}$$

and for piezoelectric ceramics, the matrix of piezoelectric d constants has the form:

$$
d = \begin{bmatrix}
0 & 0 & 0 & 0 & d_{15} & 0 \\
0 & 0 & 0 & d_{15} & 0 & 0 \\
d_{31} & d_{31} & d_{33} & 0 & 0 & 0
\end{bmatrix}
\tag{8}
$$

The piezoelectric constitutive properties are all derived relative to the material poling direction which may change throughout the volume of the piezoelectric material. In the global coordinate system, if we denote the vector representing the direction of piezoelectric poling as $p(x)$ then rotation matrices relating the local to global directions and strains can be defined:

$$S' = R_s(x,p)S \quad \text{and} \quad E' = R_E(x,p)E \tag{9}$$

where R_s is commonly used in elasticity and can be found in Cook [21], and R_E is simply a matrix of direction cosines. Given these rotations the piezoelectric properties can be written:

$$
\begin{bmatrix} D \\ T \end{bmatrix} = \begin{bmatrix} R_E^T \epsilon^s R_E & R_E^T e R_s \\ -R_s^T e_s R_E & R_s^T c^E R_s \end{bmatrix} \begin{bmatrix} E \\ S \end{bmatrix}
\tag{10}
$$

Now that the constitutive relations for both the structure and the piezoelectric materials have been defined, the strain-displacement and field-potential relations can be introduced.

$$S = L_u \mu(x) \quad \text{and} \quad E = L_\varphi \varphi(x) = -\nabla \cdot \varphi(x) \tag{11}$$

where L_u is the linear differential operator for the particular elasticity problem

and L_v is the gradient operator. It is interesting to note the symmetries between the operations on the electrical and mechanical quantities as the derivation progresses.

With the constitutive relations in hand, the fundamental assumption of the Rayleigh-Ritz formulation is introduced. The displacement and potential function can be expressed in terms of generalized coordinates:

$$u(x,t) = \Psi_r(x)r(t) = [\psi_{r_1}(x) \cdots \psi_{r_n}(x)]\begin{bmatrix} r_1(t) \\ \vdots \\ r_n(t) \end{bmatrix} \tag{12a}$$

and for the electrical potential

$$\varphi(x,t) = \Psi_v(x)v(t) = [\psi_{v_1}(x) \cdots \psi_{v_m}(x)]\begin{bmatrix} v_1(t) \\ \vdots \\ v_m(t) \end{bmatrix} \tag{12b}$$

where r_i is the generalized mechanical coordinate and v_i is the generalized electrical coordinate. It is sometimes convenient to let the v_i represent physical voltages at the piezoelectric electrodes, particularly when these are driven by a voltage amplifier.

The only limitation on the assumed displacement distributions, Ψ_{ri}, is that they obey the geometric boundary conditions while the only constraint on the assumed potential distributions, Ψ_{vi}, is that they be consistent with the prescribed voltage boundary conditions (e.g., at ground the potential $= 0$) and are equipotential at conductors. The assumed shapes should also be differentiable to the order of L_u or L_φ. Future equations will be simplified if we use strain and field basis functions:

$$S(x,t) = N_r(x)r(t) \text{ and } E(x,t) = N_v(x)v(t) \tag{13}$$

where

$$N_r(x) = L_u\Psi_r(x) \text{ and } N_v(x) = L_\varphi\Psi_v(x) \tag{14}$$

At this point, the equations of motion of the piezoelectrically coupled electromechanical system can be derived by substituting Equations (2), (4) and (10) into (1) and taking the variations:

$$\int_{t_1}^{t_2}\left[\int_{V_s} \varrho_s \partial\dot{u}^T\dot{u} + \int_{V_s} \varrho_p \partial\dot{u}^T\dot{u} - \int_{V_s}\partial S^T c_s S - \int_{V_s}\partial S^T R_s^T c^E R_s S\right.$$
$$\left. + \int_{V_s}\partial S^T R_s^T e R_s E + \int_{V_s}\partial E^T R_E^T e R_s S + \int_{V_s}\partial E^T R_E^T \epsilon^S R_E E\right.$$

$$\left. + \sum_{i=1}^{nf}\partial u(x_i)\cdot f(x_i) - \sum_{j=1}^{nq}\partial\varphi_j\cdot q_j\right]dt = 0 \tag{15}$$

The first two terms of Equation (15) can be integrated by parts in time and Equation (13) substituted in. Allowing arbitrary variations of r and v, two matrix equations in the generalized coordinates are obtained. These will be called the actuator and sensor equations of the electroelastic system.

$$(M_s + M_p)\ddot{r} + (K_s + K_p)r - \Theta v = B_f f \qquad \text{Actuator Equation} \tag{16a}$$

$$\Theta^T r + C_p v = B_q q \qquad \text{Sensor Equation} \tag{16b}$$

where the mass matrices are defined

$$M_s = \int_{V_s}\Psi_r^T(x)\varrho_s(x)\Psi_r(x) \qquad M_p = \int_{V_s}\Psi_r^T(x)\varrho_p(x)\Psi_r(x) \tag{17a}$$

and the stiffness matrices are defined (dropping the integrand's explicit spatial dependance)

$$K_s = \int_{V_s} N_r^T c_s N_r, \qquad K_p = \int_{V_s} N_r^T R_s^T c^E R_s N_r, \tag{17b}$$

the piezoelectric capacitance matrix, C_p, and electromechanical coupling matrix, Θ, are defined.

$$C_p = \int_{V_s} N_v^T R_E^T \epsilon^S R_E N_v, \qquad \Theta = \int_{V_s} N_r^T R_s^T e R_E N_v \tag{17c}$$

and finally the forcing matrices are defined

$$B_f = \begin{bmatrix} \Psi_{r_1}^T(x_{f_1}) & \cdots & \Psi_{r_1}^T(x_{f_{nf}}) \\ \vdots & & \vdots \\ \Psi_{r_n}^T(x_{f_1}) & \cdots & \Psi_{r_n}^T(x_{f_{nf}}) \end{bmatrix} \tag{17d}$$

$$B_q = \begin{bmatrix} \Psi_{v_1}(x_{q_1}) & \cdots & \Psi_{v_1}(x_{q_{nq}}) \\ \vdots & & \vdots \\ \Psi_{v_m}(x_{q_1}) & \cdots & \Psi_{v_m}(x_{q_{nq}}) \end{bmatrix} \tag{17e}$$

where there are n mechanical degrees of freedom (DOF) and m electrical DOF as well as nf forces and nq applied charges.

Equation (16) represents the general equations for an elastic body with piezoelectric material and arbitrary electrode arrangement and piezoelectric geometry. Note that the capacitance matrix as well as the mass and stiffness matrices are obtained for the piezoelectric. It is also important to remember that the physical

voltages, v_p, at the piezoelectric electrodes are related to the generalized voltage coordinates through the B_q matrix.

$$v_p = B_q^T v \quad (18)$$

This constrains the coordinates, v.

The actuator equations are those typically used to model voltage driven piezoelectric actuators. Since the voltage is commanded across the piezoelectric the capacitance and other dynamics are ignored. The sensor equations are typically used to find the voltage appearing across the piezoelectric when the structure is deformed. If there is no leakage and the electrodes are open circuited, then q is zero and the voltage appearing on the electrodes for a prescribed mechanical deflection is given by the sensor equation.

Since the rotation matrices for the piezoelectric properties are functions both of the positions within the material as well as the local poling directions, these equations are general enough to permit poling directions which vary within the volume of the piezoelectric elements.

Of particular interest is the coupling matrix, Θ. It is a function both of the piezoelectric constant and of the assumed electrical potential and mechanical displacement field shapes. In particular, for a particular mechanical mode, the designer can select electrical potential field shapes which are orthogonal by varying the electrode geometry of the piezoelectrics. Thus by varying the electrode geometry, the designer can obtain

$$\int_{v_s} N_{r_i}(x) \cdot N_{r_j}(x) = \begin{cases} 1 & i = j \\ 0 & i \neq j \end{cases} \quad (19)$$

This effect is the basis of modal sensor and actuators which work by diagonalizing the coupling matrix [11]. It demonstrates the range of possibilities available to the controls designer by varying electrode geometry.

STATE SPACE MODELS

In this section the state space models for systems with voltage or charge driven piezoelectrics will be developed both in the case of direct piezoelectric drive and indirect drive through a shunting circuit which affects the dynamics of the system. The dynamics of the piezoelectric actuator and the passive electronics can play an important part in the overall system dynamics.

Voltage Driven Electrodes

In this section the state space equations for the case of direct voltage drive of the piezoelectric electrodes will be derived. It will be assumed that the voltages at all the piezoelectric electrodes are commanded to be either zero (i.e., shorted) or some other value as a function of time. If the generalized coordinates, v, are in fact the voltages at the piezoelectric electrodes, v_p, then the matrix B_q is iden-

tity and the actuator Equation (16a) can be used to describe the dynamics of the system. In this case the system is described

$$\dot{x}_r = A^v x_r + B^v u$$
$$y = C^v x_r + D^v u \quad (20)$$

where

$$x_r = \begin{bmatrix} r \\ \dot{r} \end{bmatrix}, \quad u = \begin{bmatrix} f \\ v \end{bmatrix} = \begin{bmatrix} f \\ v_p \end{bmatrix}, \quad (21a)$$

$$A^v = \begin{bmatrix} 0 & I \\ -M^{-1}K & -M^{-1}C \end{bmatrix}, \quad B^v = \begin{bmatrix} 0 & 0 \\ M^{-1}B_f & M^{-1}\Theta \end{bmatrix} \quad (21b)$$

$$M = M_s + M_p, \quad K = K_s + K_p \quad (21c)$$

and C is an arbitrary viscous damping matrix. In this case, it is assumed that the generalized voltages correspond to physical voltages on the electrodes.

Difficulty now arises if there is not a one to one correspondence between the generalized coordinates and the physical voltages on the piezoelectric electrodes. There could conceivably be more assumed electrical potential shapes than actual electrodes on the piezoelectrics. The task now is to express the generalized voltages in terms of the commanded electrode voltages. To do this we must use the sensor Equation (16b).

$$v = -C_p^{-1}\Theta^T r + C_p^{-1} B_q q \quad (22)$$

Premultiplying by B_q^T and using Equation (18), one obtains a relationship between the voltage on the electrode, the generalized mechanical coordinates, and the applied external charges at the electrodes:

$$v_p = -B_q^T C_p^{-1}\Theta^T r + B_q^T C_p^{-1} B_q q \quad (23a)$$

which can be more simply written:

$$v_p = T_r r + T_q q \quad (23b)$$

since the v_p are specified, the q can now be obtained and substituted into (22) to give

$$v = [B_q^{T(-1)}B_q^T - I]C_p^{-1}\Theta^T r + B_q^{T(-1)}v_p \quad (24)$$

where

$$B_q^{T(-1)} = C_p^{-1}B_q(B_q^T C_p^{-1} B_q)^{-1} \quad (25)$$

is a right weighted psuedoinverse of B_q^T. The expression for v, Equation (24), can be substituted into Equation (20) and (21) to obtain the general state space matrices for voltage driven piezoelectrics.

$$A^v = \begin{bmatrix} 0 & I \\ -M^{-1}K^{sc} & -M^{-1}C \end{bmatrix}, \quad B^v = \begin{bmatrix} 0 & 0 \\ M^{-1}B_f & M^{-1}\Theta^v \end{bmatrix} \tag{26}$$

$$K^{sc} = K + \Theta(I - B_q^{T(-1)}B_q^T)C_p^{-1}\Theta^T \quad \Theta^v = \Theta B_q^{T(-1)} \tag{27}$$

The matrix K^{sc} is the system stiffness matrix with the piezoelectric electrodes short circuited. Note that Equations (26) and (27) reduce to Equations (20) and (21) in the typical case of B_q full rank.

The output equation matrices in Equation (20), C^v and D^v, are dependant on the choice of observed outputs. For illustrative purposes, it will be assumed that the desired outputs consist of the components of the displacement vector at location x, and the voltage on the ith electrode. With these assumptions the output vector, y becomes

$$y = \begin{bmatrix} u(x_s) \\ v_{pi} \end{bmatrix} \tag{28}$$

and the output matrices become

$$C^v = \begin{bmatrix} \Psi_s(x_s) & 0 \\ 0 & 0 \end{bmatrix}, \quad D^v = \begin{bmatrix} 0 & 0 \\ 0 & [0 \cdots 1 \cdots 0] \end{bmatrix} \tag{29}$$

Charge Driven Electrodes

In this section, the case when the piezoelectric electrodes are driven by an applied charge is considered. This case is easily derived from the voltage driven cases by noting that Equation (22), the sensor equation, gives the generalized voltages in terms of the applied charge. This expression can be substituted into (20) for the generalized voltages to give the charge driven state space form

$$\dot{x}_r = A^q x_r + B^q u$$
$$y = C^q x_r + D^q u \tag{30}$$

where

$$x_r = \begin{bmatrix} r \\ \dot{r} \end{bmatrix}, \quad u = \begin{bmatrix} f \\ q \end{bmatrix} \tag{31a}$$

$$A^q = \begin{bmatrix} 0 & I \\ -M^{-1}K^{oc} & -M^{-1}C \end{bmatrix}, \quad B^q = \begin{bmatrix} 0 & 0 \\ M^{-1}B_f & M^{-1}\Theta^q \end{bmatrix} \tag{31b}$$

$$K^{oc} = K + \Theta C_p^{-1}\Theta^T \quad \Theta^q = \Theta C_p^{-1}B_q \tag{31c}$$

where K^{oc} is the system stiffness with the piezoelectric electrodes open circuited.

The output equation matrices in Equation (30), C^q and D^q, are again dependant on the choice of observed outputs. As for the voltage driven case, it will be assumed that the desired outputs consist of the components of the displacement vector at location x, and the voltage on the ith electrode, Equation (28). With these assumptions, Equation (23) can be used to derive the output matrices

$$C^q = \begin{bmatrix} \Psi_s(x_s) & 0 \\ [T_v]_i & 0 \end{bmatrix}, \quad D^q = \begin{bmatrix} 0 & 0 \\ 0 & [T_q]_i \end{bmatrix} \tag{32}$$

and the subscript [ ]$_i$, indicates the ith row of the matrix and T_v and T_q are defined in Equation (23).

Mixed Voltage and Charge Specified Electrodes

In this section, the general case when some of the electrodes are voltage driven or constrained and some are charge driven or constrained will be examined. In general, each electrode of the system either has a voltage or charge boundary condition associated with it. While this is obvious if the electrode is being driven by either a voltage or charge source, even undriven electrodes have these conditions. For instance, if the electrode is shorted this corresponds to a voltage condition of $v_p = 0$; while if it is left open but unforced, this corresponds to a charge condition that $q = 0$. Thus each electrode, forced or unforced, can be classified as either voltage or charge specified.

If the charge is specified at the electrode, then the voltage at that electrode is not known a priori and vice versa for the case that the voltage is specified. A rearranged version of Equation (23) can be used to determine the unspecified quantities in terms of the specified voltages and charges and the current mechanical state of the system. Using Equation (23) and grouping the specified voltages and charges, one obtains

$$\begin{bmatrix} [v_p]_{sp} \\ [v_p]_{us} \end{bmatrix} = \begin{bmatrix} [T_v]_{sp} \\ [T_v]_{us} \end{bmatrix} r + \begin{bmatrix} [T_q]_{sp}^{us} [T_q]_{sp}^{sp} \\ [T_q]_{us}^{us} [T_q]_{us}^{sp} \end{bmatrix} \begin{bmatrix} q_{us} \\ q_{sp} \end{bmatrix} \tag{33}$$

which can be used to determine either the unspecified electrode voltages or charges. The superscript [ ]^{sp} refers to columns pertaining to charges which have been specified while the subscript [ ]$_{sp}$ refer to rows and likewise for the unspecified, us, rows and columns. Once either the unspecified voltages or charges are determined, they can be substituted into the voltage or charge driven state equations with the appropriate modification to the stiffness matrix due to the r term. In this manner arbitrary electrode forcing can be modelled.

Models of Piezoelectric Systems with Electronics

At this point, the state space equations for the piezoelectric system coupled to electronics will be developed. The electroelastic system is coupled to electronic circuitry at the piezoelectric electrodes; and the circuitry is driven by voltage and current (charge) sources as shown in Figure 3.

When there are no voltage or current sources and the electrical circuit can be represented as a network of impedances, the behavior of the elastic system is still affected by the presence of the passive electronics by virtue of the electro-mechanical coupling afforded by the piezoelectrics. The passive electronics modi-fies the dynamics of the mechanical system since the piezoelectric elements act as a transformer converting mechanical energy to electrical energy and vice versa.

This phenomenon has been applied to the problem of adding passive damping to a structure [15]. To see how this might work, consider the case of a resistor across the electrodes of a piezoelectric. As the piezoelectric deforms, a charge is generated on the electrodes which leaks through the shunting resistor dissipating energy. In essence the loss factor of the piezoelectric material has been increased by the passive shunting circuit. More complicated circuits can be connected to the piezoelectric electrodes to form resonant dampers which can in turn be tuned to structural modes in a manner directly analogous to classical mechanical vibra-tion absorbers.

In order to keep the discussion general, the shunting circuit will be char-acterized by its own state space model. The outputs of the model will be the cur-rent flowing out of the circuit at the piezoelectric electrodes as shown in Figure 3. These currents are in turn a function both of the voltage and current sources within the circuit, and the voltages at the piezoelectric electrodes. Thus the volt-ages at the electrodes as well as the sources will be considered inputs into the state space model of the electrical network. A general state space model for the electronics can be written:

$$\dot{x}_{el} = A^{el} x_{el} + [B^{el}_{I_0}\ B^{el}_{V_0}\ B^{el}_{v_p}] \begin{bmatrix} I_0 \\ V_0 \\ v_p \end{bmatrix} \tag{34a}$$

$$I_p = C^{el} x_{el} + [D^{el}_{I_0}\ D^{el}_{V_0}\ D^{el}_{v_p}] \begin{bmatrix} I_0 \\ V_0 \\ v_p \end{bmatrix} \tag{34b}$$

Once the state space model of the electrical circuitry has been obtained, it can be coupled into the model for the direct charge driven system presented in Equa-tions (30) and (31). This coupling is done by noting that I_p is the derivative of q, and that v_p is a function of q and r in Equation (23). By augmenting the state matrix with q and x_{el}, the complete model of the piezoelectrically coupled elec-tromechanical system can be written

$$\dot{x}_{sh} = A^{sh} x_{sh} + B^{sh} u_{sh}$$
$$y = C^{sh} x_{sh} + D^{sh} u_{sh} \tag{35}$$

where

$$x_{sh} = \begin{bmatrix} x_r \\ q \\ x_{el} \end{bmatrix}, \quad u_{sh} = \begin{bmatrix} f \\ I_0 \\ V_0 \end{bmatrix} \tag{36a}$$

$$A^{sh} = \begin{bmatrix} A^q & [B^q]^\cdot & 0 \\ \overline{D'}_{v_p} & D''_{v_p} & C^{el} \\ B'_{v_p} & B''_{v_p} & A^{el} \end{bmatrix}, \quad B^{sh} = \begin{bmatrix} [B^q]^\cdot & 0 & 0 \\ 0 & D^{el}_{I_0} & D^{el}_{V_0} \\ 0 & B^{el}_{I_0} & B^{el}_{V_0} \end{bmatrix} \tag{36b}$$

$$B'_{v_p} = -B^{el}_{v_p} B^T_q C^{-1}_p B_q \qquad B''_{v_p} = -B^{el}_{v_p} B^T_q C^{-1}_p \Theta^T$$
$$D'_{v_p} = -D^{el}_{v_p} B^T_q C^{-1}_p \Theta^T \qquad D''_{v_p} = -D^{el}_{v_p} B^T_q C^{-1}_p B_q \tag{36c}$$

The output equation matrices in Equation (35), C^{sh} and D^{sh}, are again depen-dant on the choice of observed outputs. As for the direct voltage or charge driven cases, it will be assumed that the desired outputs consist of the components of the displacement vector at location x, and the voltage on the ith electrode, Equation (28). With these assumptions the output matrices are

$$C^{sh} = [C^q\ [D^q]^r 0], \quad D^{sh} = [0\ 0\ 0] \tag{37}$$

and as usual the superscript [ ]^r indicates the columns associated with the vari-ables, q.

These complete dynamic equations exhibit the effect of the piezoelectric cou-pling between the mechanical and electrical systems. The coupling matrices D'_{v_p} and B'_{v_p} are clearly dependant on the piezoelectric coupling matrix, Θ, as is the matrix B^q. The coupling allows the electrical circuits to influence the mechanical system dynamics.

Current and Voltage Sources

Electrical Circuit

Elastic Structure
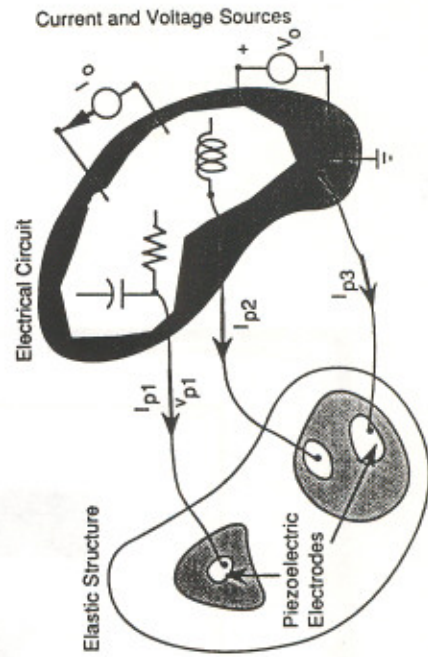
Piezoelectric Electrodes

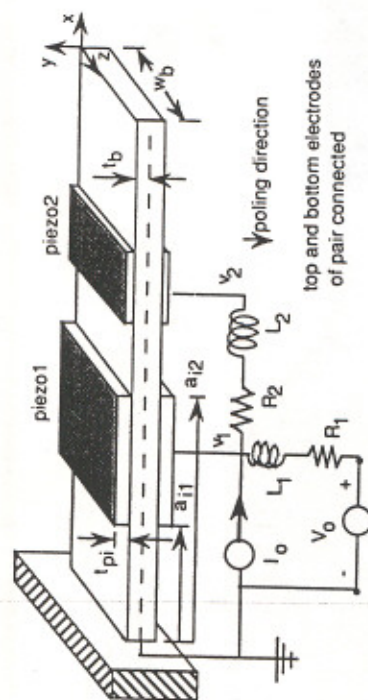*Figure 3. Electroelastic continuum coupled to voltage & current driven electronics.*

Figure 4. Assumed geometry of simple beam showing surface mounted piezoelectrics and electronics.

ILLUSTRATIVE EXAMPLE: CANTILEVERED BEAM WITH SURFACE MOUNTED PIEZOELECTRICS

In this section the general equations derived in the previous sections for the piezoelectrically coupled electromechanical systems will be applied to a simple cantilevered beam with surface mounted piezoelectrics at two locations along the beam. The configuration of the system is shown in Figure 4 with the shunting circuitry as indicated. The coordinate system is as shown with the x axis along the length of the beam and the y axis through the thickness. The poling of the piezoelectrics is in the negative y direction as shown in the figure.

The first step is to deal with the piezoelectric material property rotations. The rotation matrices are the same for each set of piezoceramics. In the convention of Equation (9), with the material polarization in the negative y direction, the electrical rotation matrices are:

$$\begin{bmatrix} E'_1 \\ E'_2 \\ E'_3 \end{bmatrix} = \begin{bmatrix} 1 & 0 & 0 \\ 0 & 0 & 1 \\ 0 & -1 & 0 \end{bmatrix}\begin{bmatrix} E_1 \\ E_2 \\ E_3 \end{bmatrix} = R_E E \tag{38a}$$

and from Reference [21] the strain rotation matrices are

$$\begin{bmatrix} S'_1 \\ S'_2 \\ S'_3 \\ S'_4 \\ S'_5 \\ S'_6 \end{bmatrix} = \begin{bmatrix} 1 & 0 & 0 & 0 & 0 & 0 \\ 0 & 0 & 1 & 0 & 0 & 0 \\ 0 & 1 & 0 & 0 & 0 & 0 \\ 0 & 0 & 0 & 0 & -1 & 0 \\ 0 & 0 & 0 & -1 & 0 & 0 \\ 0 & 0 & 0 & 0 & 0 & 1 \end{bmatrix}\begin{bmatrix} S_1 \\ S_2 \\ S_3 \\ S_4 \\ S_5 \\ S_6 \end{bmatrix} = R_s S \tag{38b}$$

At this stage assumptions must be made as to the differential operators to use in the formulation. We make the assumptions of a Bernoulli-Euler beam; and in addition, in order to increase the accuracy of the strain model within the piezoceramics, we enforce the condition that there is no stress through the thickness

of the beam or the piezoceramics. The displacement operator can be modified within the beam and piezoceramic to enforce this stress free condition.

$$S = L_u u = \begin{bmatrix} 0 & -y\dfrac{\partial^2}{\partial x^2} & 0 \\ 0 & vy\dfrac{\partial^2}{\partial x^2} & 0 \\ 0 & 0 & 0 \\ 0 & 0 & 0 \\ 0 & 0 & 0 \\ 0 & 0 & 0 \end{bmatrix}\begin{bmatrix} u_1 \\ u_2 \\ u_3 \end{bmatrix} \tag{39}$$

where ν is the Poisson's ratio of the structure or piezoceramic. Now if we assume that the electric field is constant through the piezoceramic thickness, the potential operator becomes

$$E = L_\varphi \varphi = \begin{bmatrix} 0 \\ -\dfrac{\partial}{\partial y} \\ 0 \end{bmatrix}\varphi \tag{40}$$

At this point the designer must decide upon the shapes of the assumed displacement field and electrical potential. For the displacement field we will use the first five cantilevered beam exact mode shapes in Reference [22] augmented by two additional "static" modes which represent the beam deflections if one or the other piezoceramic bending pairs has a voltage applied to it. These static mode shapes help to better represent any residual strain energy due to the discontinuous stiffness at the piezoelectrics. If a_{i_1} and a_{i_2} are the endpoints of the ith piezoceramic and u_2 is the y component of the displacement vector, u, then the static mode corresponding to that piezoceramic can be represented.

$$u''_{i_2}(x) = \begin{cases} 0 & x < a_{i_1} \\ \left(\dfrac{x - a_{i_1}}{a_{i_2} - a_{i_1}}\right)^2 & a_{i_1} < x < a_{i_2} \\ 1 + 2\dfrac{x - a_{i_2}}{a_{i_2} - a_{i_1}} & x > a_{i_2} \end{cases} \tag{41}$$

Thus the displacement vector is represented

$$u = \begin{bmatrix} 0 & 0 & 0 & 0 & 0 \\ u_1^{xx} & u_2^{xx} & u_3^{xx} & u_4^{xx} & u_5^{xx} \\ 0 & 0 & 0 & 0 & 0 \end{bmatrix} \begin{bmatrix} r_1 \\ r_2 \\ r_3 \\ r_4 \\ r_5 \\ r_6 \\ r_7 \end{bmatrix} = \Psi_r r \tag{42}$$

where the superscript $(\ )^x$ denotes the exact mode shapes.

In a like manner we can represent the potential field within the piezoceramic in terms of the voltages at the electrodes of the pairs, v_1 and v_2.

$$\varphi = [\Psi_{v_1} \quad \Psi_{v_2}] \begin{bmatrix} v_1 \\ v_2 \end{bmatrix} = \Psi_v v \tag{43}$$

where

$$\Psi_{v_i}(x) = \begin{cases} 0 & x < a_{i_1} \\[4pt] \dfrac{y - t_b}{t_{p_i}} & a_{i_1} < x < a_{i_2}, \; y > 0 \\[4pt] 0 & x > a_{i_2} \\[8pt] 0 & x < a_{i_1} \\[4pt] \dfrac{-y - t_b}{t_{p_i}} & a_{i_1} < x < a_{i_2}, \; y < 0 \\[4pt] 0 & x > a_{i_2} \end{cases} \tag{44}$$

This shape gives constant electric field in opposite directions within the upper and lower piezoceramics in a bending pair. The constant field assumption is good because the piezoceramics have uniform thickness, t_p, which is assumed thin enough to prevent significant fringe effects.

Now, substituting these matrices into Equations (17a–d) the mass, stiffness, coupling and capacitance matrices for the system can be found. After integrating over the y and z directions, the system matrices are given in terms of integrals over the length of the beam.

$$M_s = \int_0^L \rho_s A_s \Psi_r^T \Psi_r \, dx \qquad M_p = \sum_i \left(\int_{a_{i_1}}^{a_{i_2}} \rho_{p_i} A_{p_i} \Psi_r^T \Psi_r \, dx \right) \tag{45a}$$

$$K_s = \int_0^L (\Psi_r'')^T \hat{c}_s I_s (\Psi_r'') \, dx \tag{45b}$$

$$K_p = \sum_i \left(\int_{a_{i_1}}^{a_{i_2}} (\Psi_r'')^T \hat{c}_{p_i} I_{p_i} (\Psi_r'') \, dx \right) \tag{45c}$$

$$\Theta = \sum_i \left(\int_{a_{i_1}}^{a_{i_2}} (\Psi_r'')^T \hat{e}_{p_i} S_{p_i} \begin{bmatrix} \dfrac{\delta_{1i}}{t_{p1}} & \dfrac{\delta_{2i}}{t_{p2}} \end{bmatrix} dx \right) \tag{45d}$$

$$C_p = \sum_i \left(\int_{a_{i_1}}^{a_{i_2}} \begin{bmatrix} \dfrac{\delta_{1i}}{t_{p1}} \\[6pt] \dfrac{\delta_{2i}}{t_{p2}} \end{bmatrix} \epsilon_{p_i} A_{p_i} \begin{bmatrix} \dfrac{\delta_{1i}}{t_{p1}} & \dfrac{\delta_{2i}}{t_{p2}} \end{bmatrix} dx \right) \tag{45e}$$

where i is the piezoelectric index and:

$$\hat{c}_s = [-1 \; \nu_s \; 0 \; 0 \; 0 \; 0] c_s \begin{bmatrix} -1 \\ \nu_s \\ 0 \\ 0 \\ 0 \\ 0 \end{bmatrix} \tag{46a}$$

$$\hat{c}_{P_i} = [-1 \; \nu_{P_i} \; 0 \; 0 \; 0 \; 0] R_s^T c_{P_i}^E R_s \begin{bmatrix} -1 \\ \nu_{P_i} \\ 0 \\ 0 \\ 0 \\ 0 \end{bmatrix} \tag{46b}$$

$$\hat{e}_{P_i} = \begin{bmatrix} 0 \\ 1 \\ 0 \end{bmatrix} [-1 \; \nu_{P_i} \; 0 \; 0 \; 0 \; 0] R_s^T c_{P_i}^E d_{i} R_E \begin{bmatrix} 0 \\ -1 \\ 0 \end{bmatrix} \tag{46c}$$

$$\hat{\epsilon}_{P_i} = [0 \; -1 \; 0] R_E^T \epsilon_{P_i}^S R_E \begin{bmatrix} 0 \\ -1 \\ 0 \end{bmatrix} \tag{46d}$$

and

$$A_{P_i} = 2w_b \int_{t_b}^{t_b + t_{p_i}} dy, \quad S_{P_i} = 2w_b \int_{t_b}^{t_b + t_{p_i}} y \, dy, \quad I_{P_i} = 2w_b \int_{t_b}^{t_b + t_{p_i}} y^2 \, dy \tag{46e}$$

The δ_{ij} is the Dirac delta function and the integrals are evaluated at the location of piezoelectrics.

The final element yet to be computed for the complete model is the state space representation of the electronics. The task of developing the model of the shunting circuit is a simple application of Kirchhoff's voltage and current laws. The first step is to find expressions for the current going into the piezoelectric electrodes from the circuit. In the frequency domain and with the terminology of Figure 4, the currents are

$$I_2(s) = \frac{1}{L_2 s + R_2}(v_1(s) - v_2(s))$$

$$I_1(s) = I_0(s) - I_2(s) + \frac{1}{L_1 s + R_1}(V_0(s) - v_1(s)) \qquad (47)$$

which has the state space representation

$$\begin{bmatrix} \dot{x}_{e1} \\ \dot{x}_{e2} \end{bmatrix} = \begin{bmatrix} -\dfrac{R_1}{L_1} & 0 \\[2mm] 0 & -\dfrac{R_2}{L_2} \end{bmatrix} \begin{bmatrix} x_{e1} \\ x_{e2} \end{bmatrix} + \begin{bmatrix} 0 & \dfrac{1}{L_1} & -\dfrac{1}{L_1} & 0 \\[2mm] 0 & 0 & \dfrac{1}{L_2} & -\dfrac{1}{L_2} \end{bmatrix} \begin{bmatrix} I_0 \\ V_0 \\ v_1 \\ v_2 \end{bmatrix} \qquad (48a)$$

$$\begin{bmatrix} I_1 \\ I_2 \end{bmatrix} = \begin{bmatrix} 1 & -1 \\ 0 & 1 \end{bmatrix} \begin{bmatrix} x_{e1} \\ x_{e2} \end{bmatrix} + \begin{bmatrix} 1 & 0 & 0 & 0 \\ 0 & 0 & 0 & 0 \end{bmatrix} \begin{bmatrix} I_0 \\ V_0 \\ v_1 \\ v_2 \end{bmatrix} \qquad (48b)$$

The D matrix cannot typically be ignored if there is a current source. With this set of equations the complete state space model for the voltage and current driven shunted piezoelectric system, Equations (35) and (36), can be formed and used to analyze the beam dynamics.

EXPERIMENTAL VERIFICATION

Experiments were conducted to test the validity of the analytical models developed for piezoelectrically coupled electromechanical systems. The tests were designed to investigate the dynamic interaction between the structure and the electronic circuitry in both open loop and closed loop configurations.

The structural plant was the same as analyzed in the previous section, cantilevered beam with surface bonded piezoceramics and geometry as shown in Figure 5. The cantilevered beam was 29.28 cm long, 2.54 cm wide, and 3.17 mm thick. Two sets of surface mounted piezoceramics were bonded to the beam. The lower pair was located 2.46 mm from the base and extended 6.20 cm while the upper pair extended 5 cm. The piezoceramic pairs were separated by 2.15 cm.
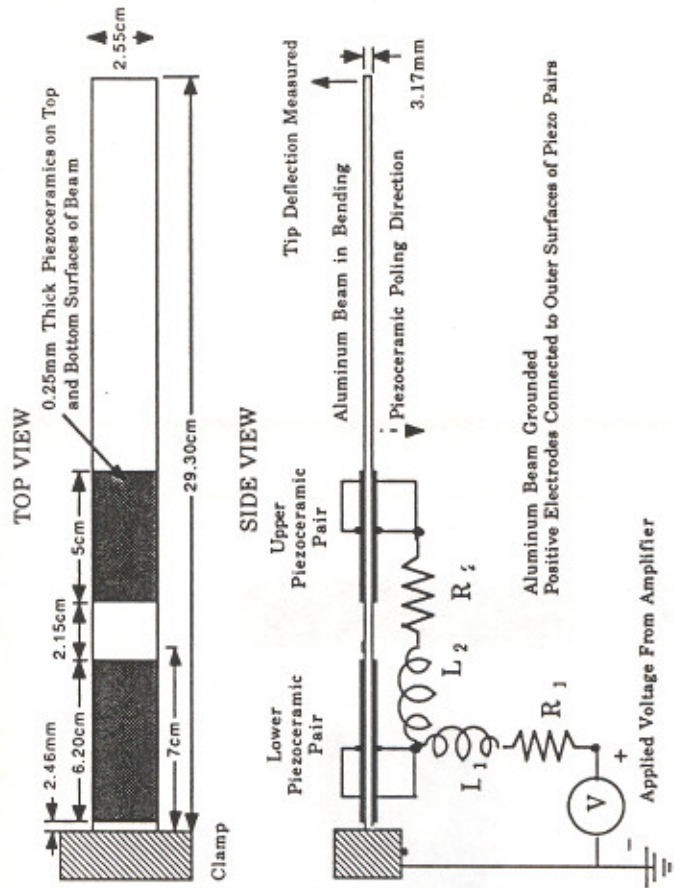
TOP VIEW

0.25mm Thick Piezoceramics on Top and Bottom Surfaces of Beam

2.55cm · 5cm · 2.15cm · 2.46mm · 6.20cm · 7cm · 29.30cm · Clamp

SIDE VIEW

Upper Piezoceramic Pair · Lower Piezoceramic Pair · Tip Deflection Measured · Aluminum Beam in Bending · Piezoceramic Poling Direction · 3.17mm · L_2 R_2 · L_1 R_1 · V · Applied Voltage From Amplifier · Aluminum Beam Grounded · Positive Electrodes Connected to Outer Surfaces of Piezo Pairs

Figure 5. Cantilevered beam test article with voltage driven electronics connecting the piezoelectric electrodes.

The piezoceramic pairs consisted of 0.25 mm thick G-1195 piezoceramic sheets manufactured by Piezoelectric Products, Inc. [23]. The pairs were poled through their thickness in the negative y direction and operating in the transverse mode. The piezoceramics were attached to the top and bottom surfaces of the beam and wired as shown in Figure 5, so as to produce a moment on the beam if a voltage were applied to either pair as described in Reference [16]. The piezoceramics are attached to the beam with a very thin layer of conducting epoxy. The beam is grounded and the positive electrodes are attached to the exterior electroded surfaces of the piezoceramic pairs. This produces opposite fields in the top and bottom piezoceramics or the pair (which are poled in the same direction), and thus causes the top piezoceramic of a pair to contract as the bottom expands, producing a moment on the beam. The material properties of the beam and the piezoceramics are presented in Table 1.

The electrodes of the piezoelectrics where connected to the passive circuit shown in Figure 5 which is the same as that modelled in Equation (48) with L_2 taken as very small. The actual values of the resistors and inductors were varied in the tests and will be described later.

The passive circuit is driven by an Apex Microsystems high voltage op-amp PA08V. The amplifier received its signal from a simple bandwidth limited dif-

Table 1. Material properties of beam and piezoelectrics.

Beam:		
Stiffness	$c_s = 73$ GPa	
Poisson's Ratio	$\nu = 0.33$	
Piezoelectric:		
Stiffness	$c_{11}^E = 63$ GPa	
	$c_{33}^E = 48$ GPa	
Poisson's Ratio:	$\nu_p = 0.40$	
Dielectric Constant	$\epsilon_3^T = 1700\epsilon^o$	
Lower	Capacitance	$C_{p1}^S = 0.156\ \mu f$
	d constants	$d_{31} = 180e\text{-}12$ m/v
		$d_{33} = 360e\text{-}12$ m/v
Upper	Capacitance	$C_{p2}^S = 0.100\ \mu f$
	d constants	$d_{31} = 276e\text{-}12$ m/v
		$d_{33} = 468e\text{-}12$ m/v

ferentiator. The setup of the signal loop is shown in Figure 6. The differentiator consisted of a zero at 2 Hz and two poles at 400 Hz on the real axis with a variable DC gain. This simple compensator was chosen, not to test performance, but simply to validate the models of the system in open and closed loop configurations. For this purpose complexity was not required.

The system input was a white noise excitation signal produced by a Tektronix 2630 data collection system. The system output is the tip deflection of the beam measured by a Bently-Nevada position sensor. In the closed loop configuration, the amplified position signal is subtracted from the command input signal coming from the Tektronix 2630. The position signal is also recorded by the Tektronix system and compared to the input.

Two type of experiments were conducted to validate the analytical models. The first type was open loop experiments to focus on the coupled dynamics of the passive electronics and the beam and to test the models for the voltage driven coupled system. In these tests, R_1 and L_1 are chosen so as to tune the electrical RLC resonance to the first beam bending mode, in accordance with Reference [15]. The values of the resistors and inductors were:

$$R_1 = 3800\Omega, \quad R_2 = 6\Omega, \quad L_1 = 94.5H, \quad L_2 = .001H \quad (49)$$

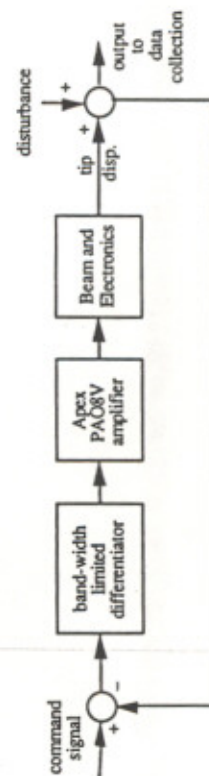The loop transfer function from input voltage to tip deflection is then measured and compared to the analytical model.

Figure 6. Experimental control loop setup.

The second type of test were closed loop experiments to focus on the utility of the state space models and the effect that the passive circuit can have on closed loop control applications. The tip displacement is fed back to the compensator as shown in Figure 6. In this test the resistor, R_1, was variable and the other circuit values were set at:

$$R_1 = 1.5 - 60 K\Omega, \quad R_2 = 6\Omega, \quad L_1 = 2H, \quad L_2 = .001H \quad (50)$$

With the dc gain of the loop set to 5000 v/v, the closed loop system is unstable unless some resistance is present at R_1. The presence of the resistance adds lag which phase stabilizes the second mode. The closed loop response is measured as a function of resistance to quantify the effects of the phase lag.

DISCUSSION OF RESULTS

The experimental transfer functions for the open loop tests with first mode resonant electronics are shown compared to the model predictions in Figure 7.
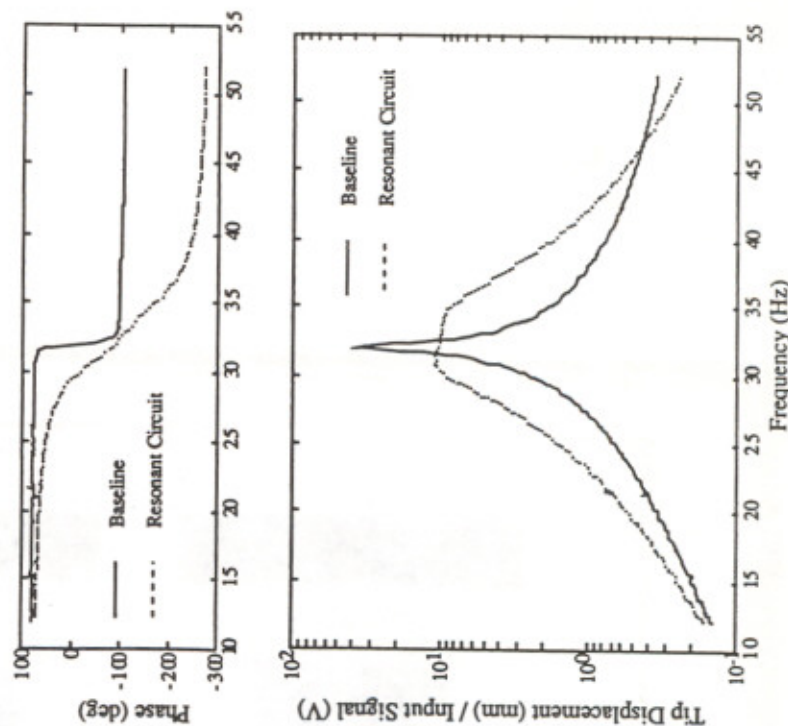

Figure 7a. Experimental first mode tip response for both the direct voltage drive (baseline) and indirect drive through a resonant circuit.
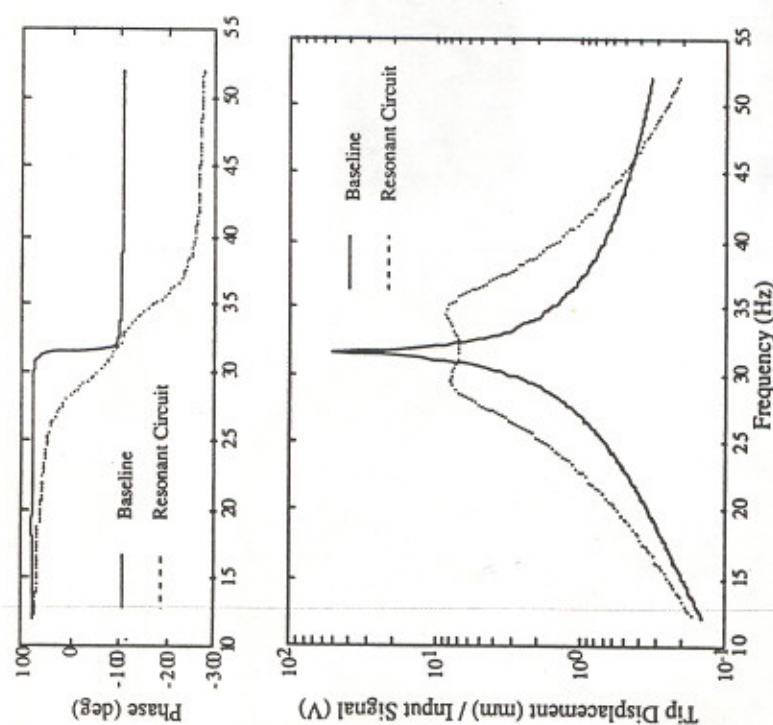
Figure 7b. Analytical first mode tip response for both the direct voltage drive (baseline) and indirect drive through a resonant circuit.

Figure 7a shows the experimental system response. The baseline case is a voltage source driving both top and bottom pairs simultaneously with shorts replacing the resistors and inductors. The resonant results have the circuit elements as described in Equation (49) with an electrical RLC resonance tuned to the first mode. Since these tests are open loop, the 10 db reduction in peak amplitude is due solely to the dynamic interaction between the electrical resonance and the beam resonance. Just as for the case of a mechanical vibration absorber, the single beam mode is replaced by two more highly damped modes [15].

The experimental results correspond rather closely to the analytical predictions shown in Figure 7b. The slight discrepancy at the peak of the transfer functions can be attributed to the difference between the model first mode frequency and that of the actual beam. The actual beam had a first natural frequency of 32.16 Hz and the Ritz model gives it at 33.36 Hz. This error will effect the predicted piezoelectric performance because the resonant circuit must be tuned to the modal frequency. The error can be partially accounted for by the large uncertainty in the piezoelectric properties. Thus, the Ritz model slightly overestimates

the amount of strain energy in the piezoceramic and therefore also the interaction between the resonant circuit and the structure. Considering the sensitivity of the performance to the exact tuning of the resonant circuit, the correlation between the model and the experiment is encouraging.

The closed loop tests were performed with the circuit parameters as in Equation (50) and R_1 variable. The DC loop gain was set at 5000 v/v for all the closed loop tests. With R_1 set below 2000Ω, the closed loop system is unstable at this value of gain. By increasing the resistance, the RC pole moves in toward the imaginary axis and adds enough phase lag to stabilize the second mode. The value of the RMS response of the closed loop system calculated over the bandwidth from 5 to 350 Hz (1st and 2nd modes) and normalized by the loop RMS response is shown compared to the analytical predictions in Figure 8. The figure shows that the relative performance of the closed loop to the open loop is maximized in the vicinity of $R_1 = 6000Ω$. Below this value the second mode contribution to the RMS response grows and above this value the first mode closed loop response grows. This is because as the resistor is increased, the RC pole acts as a low pass filter to effectively decrease the loop gain and recover the undamped first mode response.

Figure 8 shows close correlation between the analytical model and the experimental RMS response at various values of the resistance. The trends toward increased closed loop RMS response at both higher and lower resistor values than 6000Ω is clearly evident in the analytical model.
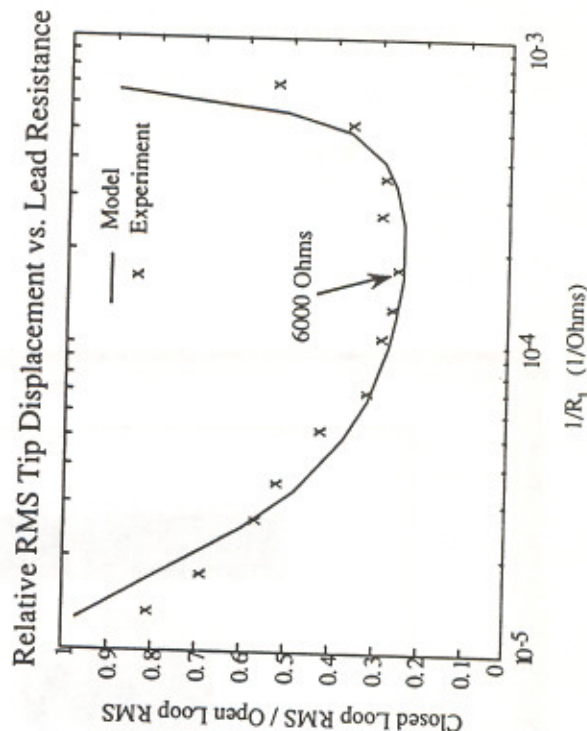
Relative RMS Tip Displacement vs. Lead Resistance

Figure 8. Comparison of relative closed loop performance as a function of resistance, R_1.

The correlation is seen even more clearly in Figure 9 where the open and closed loop transfer functions for the system with $R_1 = 6000\Omega$ are shown. The closed loop model agrees rather well in the loop transfer function with the possible exception of the zero location between the second and third mode. Zeros are difficult to model with assumed modes because they are readily influenced by the residual flexibility not captured by a finite order model.

These results suggest that the state space models for indirectly driven electromechanical systems can be effectively used to model the closed loop response of such a system. The inclusion of electrical circuitry between the source and the structure gives the designer greater ability both to model actual effects such as those caused by finite lead resistance or amplifier realities and also to modify the system dynamics to help with closed loop control.

CONCLUSIONS

The analytical models for an electroelastic continuum with piezoelectric materials coupling the mechanical and electrical coordinates were derived using an generalized version of Hamilton's principle with a Rayleigh-Ritz formulation. The piezoelectrics contribute to the mechanical mass and stiffness as well as the capacitance and electromechanical coupling of the system. The coupled equations can be thought of as actuator and sensor equations as they are typically used in these applications.

The general model was recast into state space form for voltage or charge driven electrodes. This process necessitated the use of both the actuator and sensor equations in all but the simplest case of direct voltage driven electrodes with a one to one correspondence between the number of electrodes and generalized electrical coordinates. The state space models for a system with the piezoelectric electrodes coupled to a electrical circuit were also derived. The piezoelectric's energy transformation properties highly couple the dynamics of the electrical circuit and the elastic system. This coupling can be used to add damping to structural modes or change the observability or controllability of the structure modes.

The general models were specialized to the case of a cantilevered beam to demonstrate the applications of the model to a simple structure. The predicted
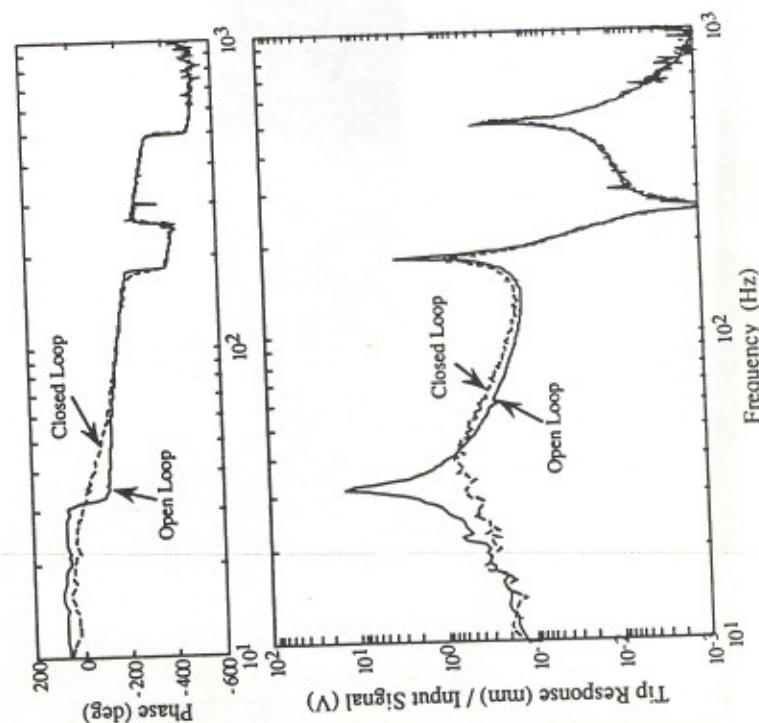

Figure 9a. Comparison of experimental open loop and closed loop response at $R_1 = 6000\Omega$.
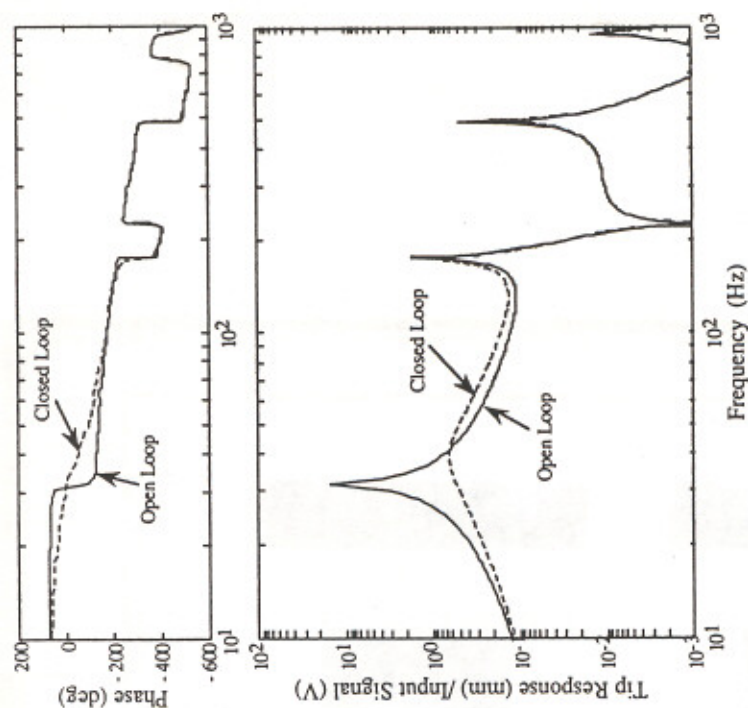
Figure 9b. Comparison of analytical open loop and closed loop response at $R_1 = 6000\Omega$.

dynamics of the beam using this model were found to be in close agreement with experiments conducted to test the model's accuracy. These non-colocated control experiments verified the predicted effects of the electrical circuit on the beam dynamics in both open loop and closed loop configuration. The experiment also demonstrated the usefulness of the actuator models in allowing the designer to modify plant dynamics in a predictable and beneficial way.

ACKNOWLEDGEMENTS

NOMENCLATURE

a_{i1}, a_{i2} = endpoints of the ith piezoelectric
A = cross sectional area
A = state dynamics matrix
B = state input matrix
B_f = generalized coordinate conversion matrix for forces
B_q = generalized coordinate conversion matrix for charges at electrodes
c = stiffness matrix
C = output matrix, or viscous damping matrix
C_p = matrix of capacitances
e_{ij} = piezoelectric material constant relating voltage in ith direction to stress in jth direction
D = vector of electrical displacements (charge/area), or direct feedthrough matrix
E = vector of electric fields (volts/meter)
$f(x_i)$ = vector of forces at location x_i
I = area moment of inertia
I_o = vector of external applied currents
K = stiffness matrix
L = generic inductor
L_u = elastic differential operator
L_v = electrical differential operator
N = matrix of differentiated shape functions, Equation (14)
q = vector of applied electrode charges
R = generic resistance
R_E = electrical field rotation matrix
R_S = engineering strain rotation matrix
S = first area moment
S = vector of material strains
t_{pi} = thickness of the piezoelectric
t_b = half thickness of the beam
T = vector of material stresses
T_e, T_s = sensor equation, simple form, Equation (23b)
$u(x)$ = vector of mechanical displacements

Modelling of Piezoelectric Actuator Dynamics for Active Structural Control

U = potential energy
v = vector of generalized electrical coordinates
v_p = vector of physical voltages at the electrodes
V_0 = external drive voltage vector
V = voltage, or volume integral
W = work function
W_e = electrical energy
W_m = magnetic energy
ϵ = matrix of dielectric constants
Θ = electromechanical coupling matrix
ν = Poisson's ratio for a material
Ψ = Matrix of assumed shape functions
ϱ = density
$\varphi(x)$ = scalar electrical potential

Subscript

el = electrical circuit
p = piezoelectric
r = mechanical coordinates
v = electrical coordinates
s = structure
t = transpose of a vector or matrix of piezoelectric material constants

Superscript

el = electrical circuitry model
E = value taken at constant field (short circuit)
D = value taken at constant electrical displacement (open circuit)
oc = open circuit
q = charge driven model
S = value taken at constant strain (clamped)
sc = short circuit
sh = coupled structure and electrical circuit model
T = value taken at constant stress (free) or transpose
v = voltage driven model
(-1) = psuedoinverse

REFERENCES

1. Crawley, E. F. and J. DeLuis. 1987. "Use of Piezoelectric Actuators as Elements of Intelligent Structures," *AIAA Journal*, 25(10):1373–1385.

2. Forward, R. L. 1979. "Electronic Damping of Vibrations in Optical Structures," *Journal of Applied Optics*, 18(5):690–697.

3. Fanson, J. L. and T. K. Caughey. 1987. "Positive Position Feedback Control For Large Space Structures," *Proceedings 28th AIAA/ASME/ASC/AHS Structures Structural Dynamics and Materials Conference*, Monterey, California, AIAA Paper No. 87-0902, pp. 588–598.

4. Hanagud, S., M. W. Obal and A. J. Calise. 1987. "Optimal Vibration Control by the Use of Piezoceramic Sensors and Actuators," *Proceedings 28th AIAA/ASME/ASCE/AHS Structures*

Structural Dynamics and Materials Conference, Monterey, California, AIAA Paper No. 87-0959, pp. 987–997.

5. Bailey, T. and J. E. Hubbard. 1985. "Distributed Piezoelectric-Polymer Active Vibration Control of a Cantilever Beam," *AIAA Journal of Guidance Control and Dynamics*, 8(5):605–611.

6. Lee, C. K. 1987. "Piezoelectric Laminates for Torsional and Bending Modal Control: Theory and Experiment,." Ph.D. Thesis, Cornell University, Ithaca, NY.

7. Fanson, J., G. Blackwood and C. Chu. 1989. "Active-Member Control of Precision Structures," *Proceedings of the 30th AIAA/ASME/ASCE/AHS Structures Structural Dynamics and Materials Conference*, AIAA Paper 89-1329.

8. Peterson, L., J. Allen, J. Lauffer, A. Miller and R. Skelton. 1989. "An Experimental and Analytical Synthesis of Controlled Structure Design," *Proceedings of the 30th AIAA/ASME/ASCE/AHS Structures Structural Dynamics and Materials Conference*, AIAA Paper 89-1170.

9. Hagood, N. W. and E. F. Crawley. 1989. "Experimental Investigation into Passive Damping Enhancement for Space Structures," *Proceedings AIAA Guidance Navigation and Control Conference, Boston, Massachusetts*, AIAA Paper No. 89-3436.

10. Spanger, R. L. 1989. "Piezoelectric Actuators for Helicopter Rotor Control," MIT Master's of Science Thesis, Dept. of Aeronautics and Astronautics.

11. Lee, C. K., W.-W. Chiang and T. C. O'Sullivan. 1989. "Piezoelectric Modal Sensors and Actuators Achieving Critical Damping on a Cantilevered Plate," *Proceedings of the 30th AIAA/ASME/ASCE/AHS Structures Structural Dynamics and Materials Conference*, Mobile, AL, pp. 2018–2026.

12. Pines, D. and A. H. von Flotow. 1990. "Active Control of Bending Wave Propagation at Acoustic Frequencies," *Journal of Sound and Vibration*, in press.

13. Miller, D. W., S. A. Collins and S. P. Peltzman. 1990. "Development of Spacially Convolving Sensors for Structural Control Applications," *Proceedings of the 31th AIAA/ASME/ASCE/AHS Structures Structural Dynamics and Materials Conference*, Long Beach, CA AIAA Paper 90-1127.

14. Edwards, R. H. and R. H. Miyakawa. 1980. *Large Structure Damping Task Report*, Hughes Aircraft Co. Report No. 4132.22/1408.

15. Hagood, N. W. and A. H. von Flotow. 1989. "Damping of Structural Vibrations with Piezoelectric Materials and Passive Electrical Networks," *Proceedings of the Damping '89 Conference*, West Palm Beach, Florida, accepted by the *Journal of Sound and Vibration*.

16. Crawley, E. F. and E. H. Anderson. 1990. "Detailed Models of Piezoceramic Actuation of Beams," *Journal of Intelligent Material Systems and Structures*, 1(1):4–25.

17. Crawley, E. F. and K. Lazarus. "Induced Strain Actuation of Isotropic and Anisotropic Plates," *Proceedings 30th AIAA/ASME/ASCE/AHS Structures Structural Dynamics and Materials Conference*, Mobile, Alabama, AIAA Paper No. 89-1326, pp. 1451–1461.

18. Crandall, S. H., D. C. Karnopp, E. F. Kurtz, Jr. and D. C. Pridmore-Brown. 1968. *Dynamics of Mechanical and Electromechanical Systems*, Robert E. Krieger Publishing Co., Malabar, Florida, pp. 291–326.

19. *IEEE Std 176-1978 IEEE Standard on Piezoelectricity*, The Institute of Electrical and Electronics Engineers, pp. 9–14 (1978).

20. Jaffe, B., R. Cook and H. Jaffe. 1971. *Piezoelectric Ceramics*, Academic Press, New York, NY.

21. Cook, R. D. 1981. *Concepts and Applications of Finite Element Analysis*, Second Edition, John Wiley & Sons, New York, p. 150.

22. Blevins, R. D. 1987. *Formulas for Frequency and Mode Shape*, Robert Krieger Publishing Co., Malabar, FL.

23. *Piezoelectric Products Company Literature*, Piezoelectric Products Inc., Metuchen, NJ (1984).